



Forecasting marine debris spill accumulation patterns in the south-eastern Australia water: an intercomparison between global ocean forecast models

Fanglou Liao¹ · Xiao Hua Wang¹ · Erick Fredj²

Received: 1 August 2022 / Accepted: 23 January 2023 / Published online: 4 February 2023
© Springer-Verlag GmbH Germany, part of Springer Nature 2023

Abstract

Forecasting transport and fates of marine debris spilled from lost ship containers is increasingly important. This paper builds a forecast framework by forcing a state-of-the-art particle-tracking model with operational oceanic and atmospheric forecasts, and compares simulations with the spotted debris from an actual maritime container spill in the south-eastern Australia water. In coastal areas, patterns of the spotted debris can be approximately simulated when applying surface current forecasts of an eddy-resolving resolution, along with the horizontal dispersion, Stokes drift and windage. The strengths and shortcomings of various forecast datasets varied. Therefore, a thorough analysis of various forcing datasets might be required when performing a marine debris forecast. The horizontal dispersion coefficient can be used to parameterize the unresolved small-scale processes. Stokes drift and windage, especially the latter one, can be important for the debris movements. This study suggests that some global forecast models can be used with certain confidence to forecast debris movement, however, not all are equivalent and cautions are warranted.

Keywords Marine debris · Container spill · Particle-tracking

1 Introduction

A wide variety of human-made objects (glass, plastic, ceramic, metal) enter waterways and ultimately become marine debris (Ebbesmeyer et al. 2012; Yoon et al. 2010). Marine debris has been globally recognized as a major cause for concern, especially marine plastic debris (MPD) due to its persistence, abundance and mobility (Critchell et al. 2019; United Nations Environmental Programme 2022). An estimated 5–13 million tonnes

of plastic waste entered the global ocean in 2010 from 192 countries; this amount was projected to increase by an order of magnitude by 2025 (Jambeck et al. 2015; Zhang 2017). MPD accounts for 60–80% of all marine debris (Barnes et al. 2009; Derraik 2002; Kako et al. 2014; Lebreton et al. 2012). Most MPD come from the land, transported especially by large rivers (Schmidt et al. 2017; Lebreton et al. 2017) and is mostly trapped in coastal areas, with around 52% of river-sourced plastic accumulating in the river-dominated coasts (Harris 2020). Additionally, fisheries and shipping also produce MPD (Díaz-Torres et al. 2017). The International Maritime Organization (IMO), governments and marine insurers have estimated that on average around 1380 shipping containers were lost at sea each year over the period 2008–2019 (World Shipping Council 2020). These marine incidents can significantly increase the MPD in both the open ocean and coastal areas. Actions at the local, regional and global levels are needed to curb the MPD. The increasing ability to predict environmental conditions and the fate or behaviour of MPD can provide a better support for decision-making in emergencies, and in planning responses to marine plastic

This article is part of the Topical Collection on the *12th International Workshop on Modeling the Ocean (IWMO)*, Ann Arbor, USA, 25 June–1 July 2022

Responsible Editor: Yasumasa Miyazawa

✉ Fanglou Liao
fanglou.liao@unswalumni.com

¹ The Sino-Australian Research Consortium for Coastal Management, School of Science, The University of New South Wales, Canberra, Australia

² Department of Computer Science, Jerusalem College of Technology, Jerusalem, Israel

pollution and risk management (González-Fernández and Hanke 2017).

MPD causes significantly negative impacts, including aesthetic damage to local tourism, ‘ghost fishing’ entanglement, and injury to marine biota by ingestion, physical damage and behavioural changes (Barnes et al. 2009; Bravo et al. 2009; Derraik 2002). Moreover, marine microplastics, partially from degraded macroplastics (Browne et al. 2009), can enter the food chain and threaten human health (Keswani et al. 2016; Rochman et al. 2015). Therefore, it is necessary to understand the distribution and fates of MPD on different spatiotemporal scales (Critchell et al. 2019), especially in the coastal environments on which a large population rely.

Many efforts have been taken to understand the transport of MPD in the marine environment. By applying a two-dimensional (2D) advection–diffusion model to the north-eastern coast of Australia, Critchell and Lambrechts (2016) found that factors, such as diffusivity, wind shadow (a place where the wind does not reach) created by high islands and the source location, play key roles in the fate of marine plastics. Lermusiaux et al. (2019) modelled the plastic pollution in Massachusetts Bay and emphasized the importance of dynamic processes, such as the wind-driven current, Lagrangian coherent structures (LCSs) and internal tides in the motions of plastics. Additionally, ocean surface waves can affect the movement of marine plastics at the sea surface. In particular, the Stokes drift (the net drift that a particle moving in a fluid experience in the direction of propagation of the fluid’s wave field) may be a dominant factor in the transport of floating objects (Breivik and Allen 2008; Dobler et al. 2019; Trinanés et al. 2016). For example, Dobler et al. (2019) showed that the Stokes drift can radically change the fates of floating particles in the South Indian Ocean, causing them leak to the South Atlantic Ocean rather than to South Pacific Ocean. Likewise, van der Mheen et al. (2019) examined the influences of the ocean currents, waves and wind on the buoyant plastic accumulation in the South Indian Ocean. They showed that the accumulations of MPD are highly sensitive to the applied forcing. For example, both the Stokes drift and windage (a force created on an object by friction when there is a relative movement between the air and the object) are key factors controlling the accumulations of MPD in the subtropical South Indian Ocean. Onink et al. (2018) examined the influences of various physical processes on the accumulation of floating microplastic globally. Their simulations showed that the Ekman currents to a great extent determine the accumulation zones of microplastic on the global scale. The Stokes-drift velocity and geostrophic currents do not produce marked influences on the large-scale microplastic accumulation in the subtropical oceans in their study. However, the Stokes drift increases the transport of microplastics to the Arctic regions.

However, very limited attention has been paid to MPD from ship containers lost overboard. Considering the increasing marine incidents and increasingly serious marine plastic pollution, it was felt that building a forecast framework that can make a reliable prediction on the transport of MPD spilled from lost containers is of urgent importance. Preferably, such a forecast framework can be validated by the available observations of MPD from an actual maritime incident. In this study, we built a particle-tracking forecast framework and assessed capabilities of different widely used forecast currents in simulating transport of floating MPD, taking advantage of available observational patterns of marine debris. The remainder of this manuscript is set out as follows. ‘Section 2’ describes the Yang Ming Efficiency (hereinafter YM, the name of a container ship) incident and related information on the debris, forcing datasets and the particle-tracking model. Additionally, design of numerical experiments is also described. In ‘Section 3’, we discuss the simulation results with an emphasis on an intercomparison and comparing with observations. This is followed by a summary of the principal findings and discussion on the limits of this study.

2 Data, TrackMPD and design of numerical experiments

2.1 Yang Ming Efficiency incident

Around 00:30 AM of June 1, 2018 (local time), a Liberian-flagged container ship named Yang Ming Efficiency, travelling from Taiwan to Port Botany, lost more than 80 containers overboard at 152°04.4' E, 33°01.6' S, about 30 km southeast of Newcastle. The spill was likely to be caused by a sudden and heavy rolling under rough sea conditions (AMSA Annual Report, 2018–2019; ATSB 2020); the simulated significant wave height at the time and location of the container spill was about 5.4 m (Fig. 1a). Figure 1 shows the location of the YM incident, the significant wave height (SWH) when the containers fell overboard. The red dots in Fig. 1b represent the spotted debris over the first 16 days after the YM incident. To facilitate interpreting the results, we divide the coastline into seven regions (R1–R7, Fig. 1b). It can be seen that debris was mostly spotted in R3–R6, and there was some debris in R2.

Litter washed ashore (red dots in Fig. 1b) soon after the spill (AMSA Annual Report, 2018–2019). Typical debris included nappies, rubber mats, home furnishings, toilet-paper packaging, food-packaging items, sanitary products and surgical masks. Some remained in the sunken containers and was salvaged by AMSA (Irving from AMSA, pers. Comm, 2022). More than 1000 m³ of debris was recovered and disposed of from the affected areas during the

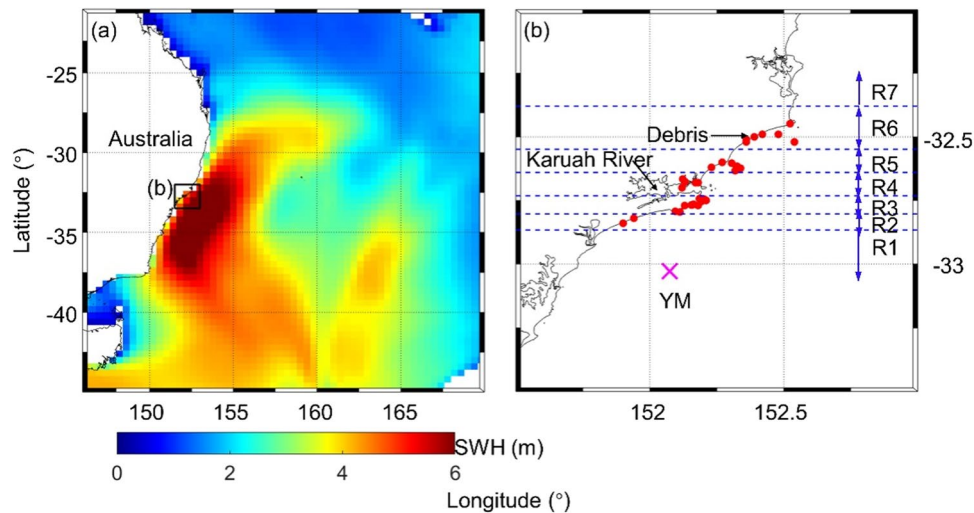


Fig. 1 (a) Significant wave height (SWH) off the east coast of Australia in the early morning of June 1, 2018 and (b) locations of YM incident (magenta cross), spotted debris (red dots) and region division (blue dash lines). Note that the spotted debris is a collection of spotted debris for the first 16 days after the YM incident (same in other

figures). Black box in (a) denotes the domain of (b). The division of these seven regions R1–R7 are mainly based on the density distribution of spotted debris. Panel (a) shows the simulation domain. Horizontal axis: longitude (°); vertical axis: latitude (°)

Table 1 A short summary of the surface current datasets. n/a means not applicable

	Bluelink	HYCOM	FOAM	MOGPR
Horizontal resolution (°)	0.1	0.083	0.25	0.25
Temporal resolution (hours)	3	3	1	3
Atmospheric forcing	ACCESS-G	NAVDEM	CALOSIM	ECWMF ERA5
Forecast (days)	7	7	10	n/a

initial response actions in 2018. Most debris concentrated on a small number of sandy beaches to the north of the spill (ATSB 2020). The information of locations of spotted debris from YM was archived by Australian Maritime Safety Authority (AMSA) and available at <https://www.amsa.gov.au/>. AMSA, however, did not archive information about the beaching time of these spotted debris. These spotted debris consisted of both plastic and non-plastic objects, and were not necessarily floating ones. That is, some spotted debris might be of neutral or negative buoyancy and moved or sunk in the subsurface water. However, in this study, we run the two-dimensional (2D) simulations and thus consider only floating macro-debris (both plastic and non-plastic).

2.2 Surface current datasets

In the forecast of the motions of floating marine debris, the surface current is one of the major forcing. Four surface current datasets are used in this study. This is primarily to test the relative performance and feasibility of different datasets in the simulation of debris transport in the YM incident. These four datasets are Bluelink, Hybrid Coordinate

Ocean Model (HYCOM), Forecast Ocean Assimilation Model (FOAM) within the European Copernicus Marine Environment Monitoring Service (CMEMS) and MULTIOBS_GLO_PHY_REP_015_004 (MOGPR) within the CMEMS. A preliminary introduction to these datasets is as follows, and readers are referred to the corresponding references for details. Table 1 provides a short summary of the four datasets.

- (1) Bluelink is an Australian platform developed by multiple organizations to model the ocean conditions, especially for the waters around Australia. There is an operational forecast system called the Ocean Modelling, Analysis and Prediction System (OceanMAPS3.0, used in this study), implemented at the Bureau of Meteorology (Brassington et al. 2007). OceanMAPS is based on a quasi-global configuration OFAM3 (Ocean Forecasting Australia Model version 3; Oke et al. 2012). A 7-day forecast at a horizontal resolution of 0.1° around Australia is publicly available, with a temporal resolution of 3 h for the variables at the sea surface. In the forecast cycle, the model is forced by the atmospheric forcing from the Australian Community Climate and

Earth-System Simulator-Global (ACCESS-G). Observations from the satellite altimetry, Array for Real-Time Geostrophic Oceanography (Argo), in situ profiles and satellite sea surface temperature (SST) were assimilated using Enkf-C software in Ensemble Optimal Interpolation (EnOI) mode. Tides are not included.

- (2) HYCOM is also a platform from multi-institutional efforts (Cummings 2005; Cummings and Smedstad 2013; Helber et al. 2013). Under HYCOM, there is a Global Ocean Forecasting System (GOFS) implemented at Naval Research Laboratory (NRL). In this study, we used GOFS version 3.1, which provides a 7-day global forecast at a horizontal resolution of 0.083° and a temporal resolution of 3 h at the sea surface. The atmospheric forcing comes from the Navy Global Environmental Model (NAVGEM). Observations from the satellite altimeter, satellite, and in situ sea surface temperature (SST) as well as in situ vertical temperature and salinity profiles from XBTs, Argo floats and moored buoys, were assimilated in a 3D variational scheme based on the Navy Coupled Ocean Data Assimilation (NCODA) system. Tides are not included.
- (3) FOAM (Blockley et al. 2014; Lea et al. 2015) is an operational ocean analysis and forecast system implemented at Met Office, UK. The version we used is a weakly coupled ocean–atmosphere data assimilation and forecast system (Lea et al. 2015). The ‘weakly’ coupling means that ‘the coupled model is used to provide background information for separate ocean–sea ice and atmosphere–land analyses. The increments generated from these separate analyses are then added back into the coupled model’ (Lea et al. 2015). The dynamical core of the ocean component is Nucleus for European Modelling of the Ocean (NEMO) v3.4 ocean model. The Coupled Atmosphere–Land–Ocean–Sea Ice Model (CALOSIM) provides the surface flux for the ocean component. The FOAM system provides a 10-day forecast at a horizontal resolution of 0.25° . The temporal resolution of the surface variables is 1 h. For the ocean and sea ice, a variational data assimilation scheme of NEMO called NEMOVAR was used. The assimilated observations include the in situ and satellite SST data, satellite altimeter sea level anomaly (SLA) data, satellite sea ice concentration data, and in situ temperature and salinity profiles from various sources including Argo, moored buoys, and temperature profiles from XBTs and marine mammals. Tides are not included.
- (4) MOGPR provides the total currents at the surface. The total currents consist of the geostrophic currents derived from the satellite measurements and the Ekman currents calculated from the ECMWF ERA5 wind

Table 2 Major settings of numerical experiments. \checkmark means inclusion and / means exclusion. The four sources of the surface current are Bluelink, HYCOM, FOAM and MOGPR. ADV, advection process only (baseline); DSP, dispersion added on top of ADV; STD, Stokes drift added on top of DSP; WDA, windage added on top of STD

	ADV	DSP	STD	WDA
Surface current	\checkmark	\checkmark	\checkmark	\checkmark
K_h (m ² /s)	/	5, 50, 100, 200	5, 50, 100, 200	5, 50, 100, 200
Stokes drift	/	/	\checkmark	\checkmark
Windage	/	/	/	1–5%

stress. The horizontal resolution is 0.25° and the data is available at a frequency of 3 h.

In this study, we compare the modelled particle trajectories with the locations of spotted debris. In general, an ultra-high-resolution hydrodynamical model is desirable to better resolve the small-scale nearshore processes and therefore the beaching of plastic debris. The highest resolution of forcing used in this study is around 8 km. This large grid size limits the model performance in forecasting beaching. Therefore, the simulated beaching in this study may only represent a chance of beaching. For example, a high density of simulated beaching particles may only suggest a high chance of beaching in the actual situation.

2.3 Surface waves and stokes drift

Not only the force from the current, but also the force due to the wind and wave also determines the motions of drifting objects (Anderson et al. 1998). Due to unavailability of the wave forecast in this region, we therefore use a hindcast of Stokes drift to investigate its effects on the trajectories and fates of debris. The hourly Stokes-drift velocity and significant wave height used in this paper are products of the Collaboration for Australian Weather and Climate Research (CAWCR), provided by the Australian Bureau of Meteorology. This wave hindcast is a global hindcast with a focus on the Australian and Pacific regions (Durrant et al. 2014), and we extracted the data for our simulation period. It is forced by the surface winds from the Climate Forecast System Reanalysis (CFSR; Saha et al. 2010) and the Climate Forecast System version 2 (CFSv2; Saha et al. 2014). Validation of the 4-arc-minute-resolution grid showed an excellent agreement with data from buoys and altimeters in the Australian region (Hemer et al. 2017). In this study, we used the wave data as part of the weather conditions when YM lost its containers (Fig. 1a), and to examine the impact

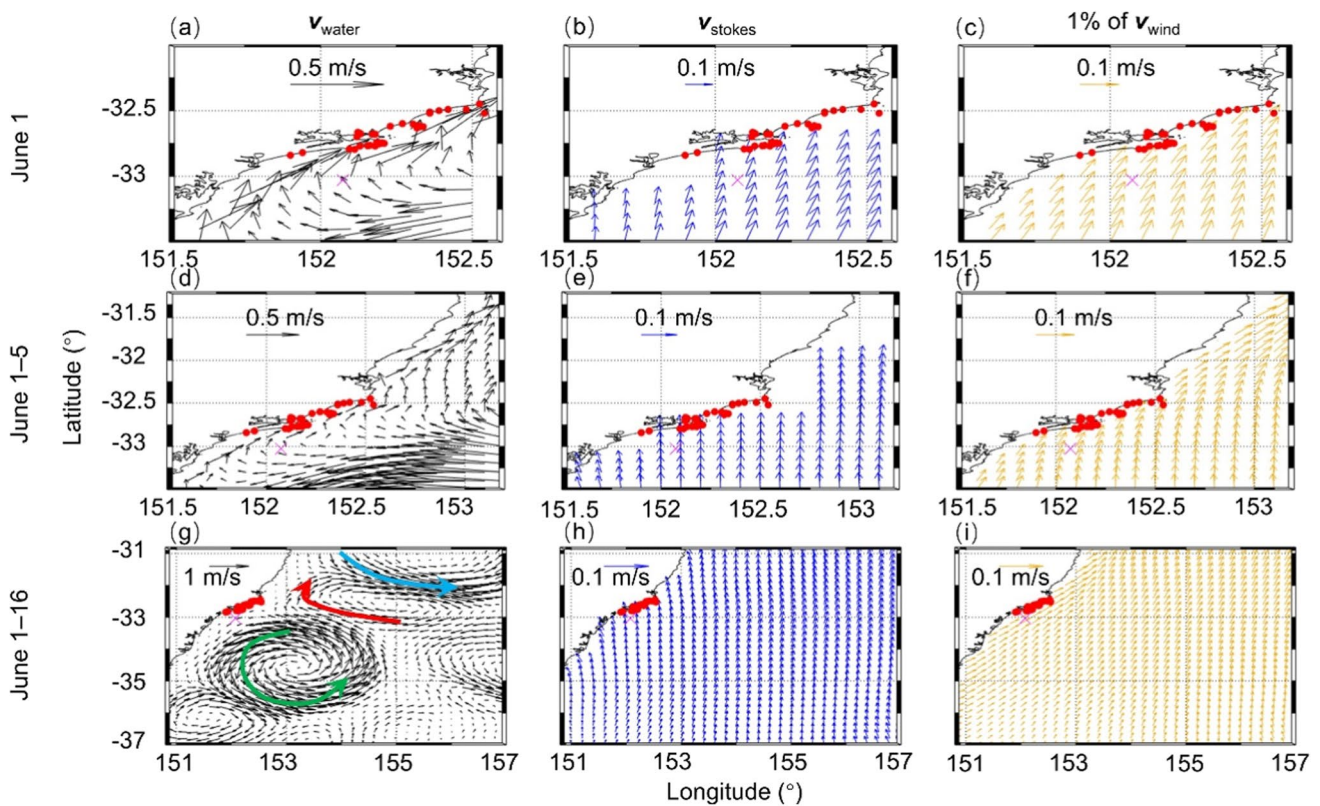


Fig. 2 Bluelink surface current (left-hand column), Stokes drift (middle column) and windage (right-hand column) averaged for the first day (top row), first 5 days (middle row) and first 16 days (bottom row) after the YM incident. Magenta cross: YM site. Green curve with arrow: anti-cyclonic mesoscale eddy. Red curve with arrow: oval cyclonic mesoscale eddy. Blue curve with arrow: branch of the

EAC separating from the coast and flowing eastward. The absence of Stokes drift data near the coastline is due to its grid resolution. For a better visualization, automatic scaling is adopted to plot the arrow. Note that the scaling factor is 1 for (b), (c), (e) and (f), but 2.5 for all other panels. Horizontal axis: longitude (°); vertical axis: latitude (°). The spatial domain is the same for each row but different among rows

of Stokes drift on the transport of the debris (Table 2). To combine it with the surface current, the Stokes-drift velocity was interpolated onto the grid of the corresponding surface current datasets (Bluelink, HYCOM, FOAM and MOGPR), and was added as a velocity component to the surface current (Eq. 1), as in prior studies (Dobler et al. 2019; Onink et al. 2018; Van Sebille et al. 2019). Subject to its grid resolution, the Stokes drift data may not be available in the vicinity of the coastline (Fig. 2).

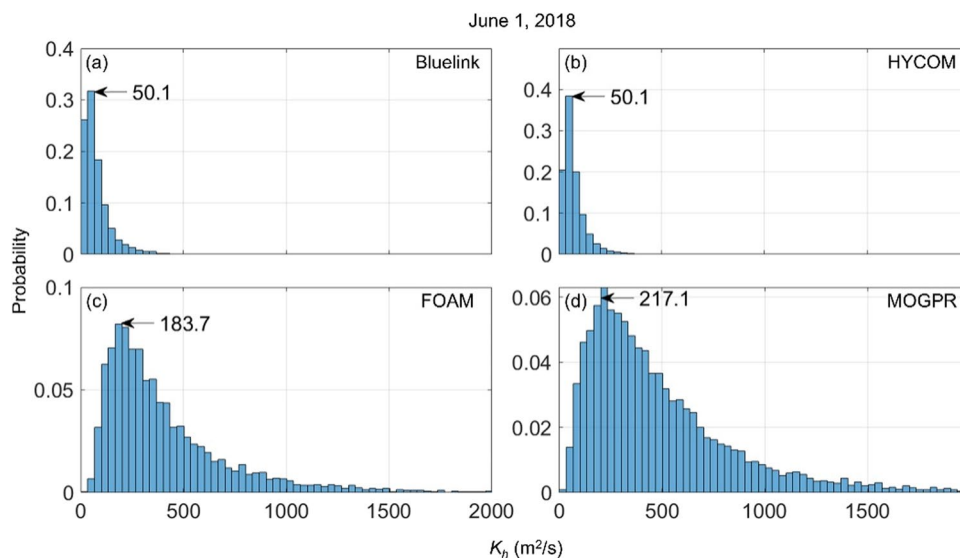
2.4 Windage

The windage, also known as the wind drift, may also affect the transport of floating marine debris, particularly for highly buoyant macro-debris. To explore the impact of the windage on the floating debris from the YM incident, a fraction α of the wind velocity v_{wind} was added to the surface current velocity v_{water} and Stokes-drift velocity v_{stokes} to give v_t , the total current to force the debris transport (Case WDA in Tab. 2). This is similar to Critchell et al. (2015) and Abascal et al. (2009).

$$v_t = v_{water} + v_{stokes} + \alpha \cdot v_{wind} \tag{1}$$

α , the windage coefficient, is directly linked to the buoyancy of the debris. As this paper focuses on different types of floating debris, it is impossible to define a precise buoyancy value that applies to all debris. We therefore selected 5 possible α values ranging from 1 to 5% at an interval of 1% (Table 2), following prior studies (Beegle-Krause 2001; Carson et al. 2013; Critchell et al. 2015). The 3-hourly wind velocity data is from the NOAA/NCEP Global Forecast System (GFS) numerical weather prediction model, at a horizontal resolution of 0.5°. We used the forecast wind velocity over the period June 1–16, 2018 for our simulation. Similar to the Stokes-drift velocity, the windage velocity was also interpolated onto the grid of the corresponding surface current datasets (Bluelink, HYCOM, FOAM and MOGPR). The primary reason for choosing the GFS forecast wind, rather than from the wind forcings for the Bluelink, HYCOM and FOAM (ECMWF ERA5 used for MOGPR is not a forecast wind but a reanalysis), is to avoid any potential bias towards a model forced by its corresponding wind stress. It is worth

Fig. 3 Histogram of K_h calculated using the surface current on June 1, 2018, based on the Smagorinsky scheme. The values with an arrow in each panel denote the K_h with the highest frequency



mentioning that the windage coefficient can be measured, for instance, in Breivik et al. (2011). Additionally, a crosswind component may be needed for objects that have no radial symmetry, although the downwind component (considered in this study) dominates in most cases. In this study, to avoid an overly wide parameter regime, we neglect the crosswind component.

The surface current v_{water} from BlueLink, Stokes-drift velocity v_{stokes} and windage velocity ($\alpha = 1\%$) averaged over the first day, first 5 days and first 16 days after the YM incident are shown in Fig. 2. The surface current was flowing westward at the YM incident site on June 1 (Fig. 2a). Along the coast, there was a strong north-eastward current. Both the Stokes-drift velocity (Fig. 2b) and windage velocity (Fig. 2c) were approximately in the north-eastward direction on June 1. Over the first 5 days, the averaged alongshore current remained in the north-eastward direction (Fig. 2d). The Stokes-drift velocity (Fig. 2e) was approximately in the northward direction and the windage velocity (Fig. 2f) was in the north-eastward near the coast. Southeast of the YM site, there was a strong anti-cyclonic eddy (Fig. 2g, green arrow). Additionally, there was a cyclonic eddy (Fig. 2g, red arrow) to the north of the anti-cyclonic eddy. The East Australian Current (EAC) approximately separates from the coast at around 31°S (Fig. 2g, light blue arrow). Over the first 16 days, the averaged Stokes-drift velocity (Fig. 2h) and windage velocity (Fig. 2i) remained northward and north-eastward, respectively. Fig. S1 shows the comparisons of the surface currents among different surface current datasets.

2.5 TrackMPD and horizontal dispersion

Track Marine Plastic Debris (TrackMPD) is a state-of-the-art particle-tracking model (Jalón-Rojas et al. 2019a, b). In

this study, the 2D version of TrackMPD (<https://github.com/IJalonRojas/TrackMPD>) was forced by the surface currents (BlueLink, HYCOM, FOAM and MOGPR), the CAWCR Stokes drift and GFS wind. The turbulent dispersion ensures that released particles spread out and therefore move under different hydrodynamical conditions. In TrackMPD, the horizontal turbulent dispersion is represented by the white-noise random walks with an average of 0 and standard deviation of 1, respectively (Jalón-Rojas et al. 2019b). A particle is considered to be ‘beached’ if it reaches the shoreline. We set the timestep of the particle tracking to be 3 h, which is the output frequency of BlueLink, HYCOM and MOGPR.

The horizontal dispersion coefficient K_h is a key parameter when running TrackMPD and is used to parameterize subgrid-scale processes unresolved by the models. From this perspective, inclusion of a K_h can be considered as the implementation of a physical process. In this study, K_h was calculated following the Smagorinsky scheme (Smagorinsky 1963), as there was no measured K_h available in our case. Figure 3 presents the histogram of the time-averaged K_h for the first day from the four current models. The time-averaged K_h for the first 5 and 16 days are similar to K_h for the first day in each dataset (not shown).

There are distinct differences between the eddy-resolving datasets (BlueLink and HYCOM) and the eddy-permitting datasets (FOAM and MOGPR). The highest frequency of K_h appears at around $50\text{ m}^2/\text{s}$ in BlueLink and HYCOM, but at around $200\text{ m}^2/\text{s}$ in FOAM and MOGPR. The largest K_h even reaches around $2000\text{ m}^2/\text{s}$ in FOAM and MOGPR. K_h can also be calculated empirically. For instance, K_h was calculated using the subgrid size and the turbulent dissipation rate (Peliz et al. 2007). A subgrid size of 10 km and a dissipation rate of $10^{-9}\text{ m}^2/\text{s}^3$ correspond to a K_h of around $215\text{ m}^2/\text{s}$, and a smaller subgrid size corresponds to

a smaller K_h . Furthermore, ASCE (1996) showed a typical range of K_h between 1 and 100 m²/s. A similar range of K_h was also calculated using stochastic methods (Carlson et al. 2010; Okubo 1971). Based on the empirical experience of slick drifts and object drifts over years or unpublished experiments (Irving, pers. comm., 2022), ambient conditions (around the considered domain) generating K_h values in excess of 50 m²/s are rare. A value of 200 m²/s is at a level of hurricane strength and that never occurred. Winds in the area over that period never exceeded 40 knots. Therefore, we set the upper limit of K_h to be 200 m²/s in our simulation.

2.6 Design of numerical experiments

Four cases with a progressive inclusion of physical processes were designed. Table 2 presents a short summary of the major settings of the numerical experiments conducted in this study. For each of the following described simulations, we repeated four times with each of the four surface current datasets, but with all other settings (horizontal dispersion, Stokes-drift velocity and windage) the same.

- (1) Case ADV is a single simulation forced by the surface current only.
- (2) Case DSP is a group of 4 simulations (4 different K_h) forced by the surface current and horizontal dispersion, with four representative K_h values: 5, 50, 100 and 200 m²/s.
- (3) Case STD is similar to case DSP but includes the Stokes-drift velocity.
- (4) Case WDA consists of 20 simulations (4 different K_h and 5 different α) with all the forcings from the case STD plus windage, with a α varying from 1 to 5% at an interval of 1%. It is worth mentioning that TrackMPD allows to activate the windage process for the spherical and cylindrical objects, but this requires the density of the objects and therefore was not applied in this paper.

The simulations are labelled based on the forcing. For example, ADV is the single simulation in the case ADV, with only the surface current included; DSP_ K_h 50 is a simulation in the case DSP with $K_h = 50$ m²/s; STD_ K_h 100 is a simulation in the case STD with $K_h = 100$ m²/s; and WDA1p_ K_h 200 is a simulation in the case WDA with a windage coefficient α of 1% (denoted by 1p; similarly, 2p stands for $\alpha = 2\%$) and $K_h = 200$ m²/s. All the simulations covered a period of 16 days from June 1, 2018, when the YM incident occurred, to 16 June, 2018, over which the spatial distribution of spotted debris locations was used in this study. This 16-day period is believed to be long enough, as a maritime search and rescue (SAR) generally extends from less than 1 day to a few days (Brushett et al. 2016), with

most coastal spill response operations concluding within weeks (Irving, pers. comm., 2022).

To avoid the random behaviour induced by the horizontal dispersion affecting the evaluation of the influences of other physical processes (e.g. Stokes drift), the displacement due to the horizontal dispersion was calculated before the main calculation loop of TrackMPD, so that the scenarios with the same coefficient K_h in cases DSP, STD and WDA had the same random displacements. This allowed us to isolate the effects of the Stokes drift and windage and is the primary reason why we did not adopt the spatiotemporal varying K_h but a few discrete K_h .

A total of 16,000 virtual particles were released simultaneously at 00:30 AM of June 1, 2018, in each numerical simulation. This number of released particles was determined by a group of sensitivity experiments (not shown), which showed a further increase of released particles to 32,000 produced very minor influence on the simulation results. To consider the uncertainties in the initial spill site (YM shown in Fig. 1), we generated an array of random number with an average of 0 and standard deviation of 0.01. These numbers were added as an initial position error (no greater than 0.01°) in both the longitude and latitude directions.

3 Simulation of particle trajectories and comparison with observations

3.1 On June 1, 2018

A first-day forecast is essential for a fast response to a maritime incident. In this subsection, we present simulations forced by different forcings with a fixed K_h of 50 m²/s, and compare the simulated patterns of particle distribution with spotted debris.

3.1.1 Spatial distribution of the released particles

Bluelink (Fig. 4a) or HYCOM (Fig. 4b) surface current can force these particles move in the north-eastward direction, similar to the surface current direction (Fig. S1). By the end of June 1, 2018, particles moved much farther when forced by the HYCOM surface current and arrived at around 32.6°S, but at around 32.8°S under the forcing of Bluelink surface current. The spread of these particles in the first row (without horizontal dispersion) of Fig. 4 is due to the small fluctuations in the initial release site. These particles entered the region where debris from YM was spotted, especially when forced by the HYCOM surface current, mostly in R5. When forced by FOAM (Fig. 4c) or MOGPR (Fig. 4d) surface current, these particles moved in the eastward or westward direction, respectively, and no particle entered the region where debris was

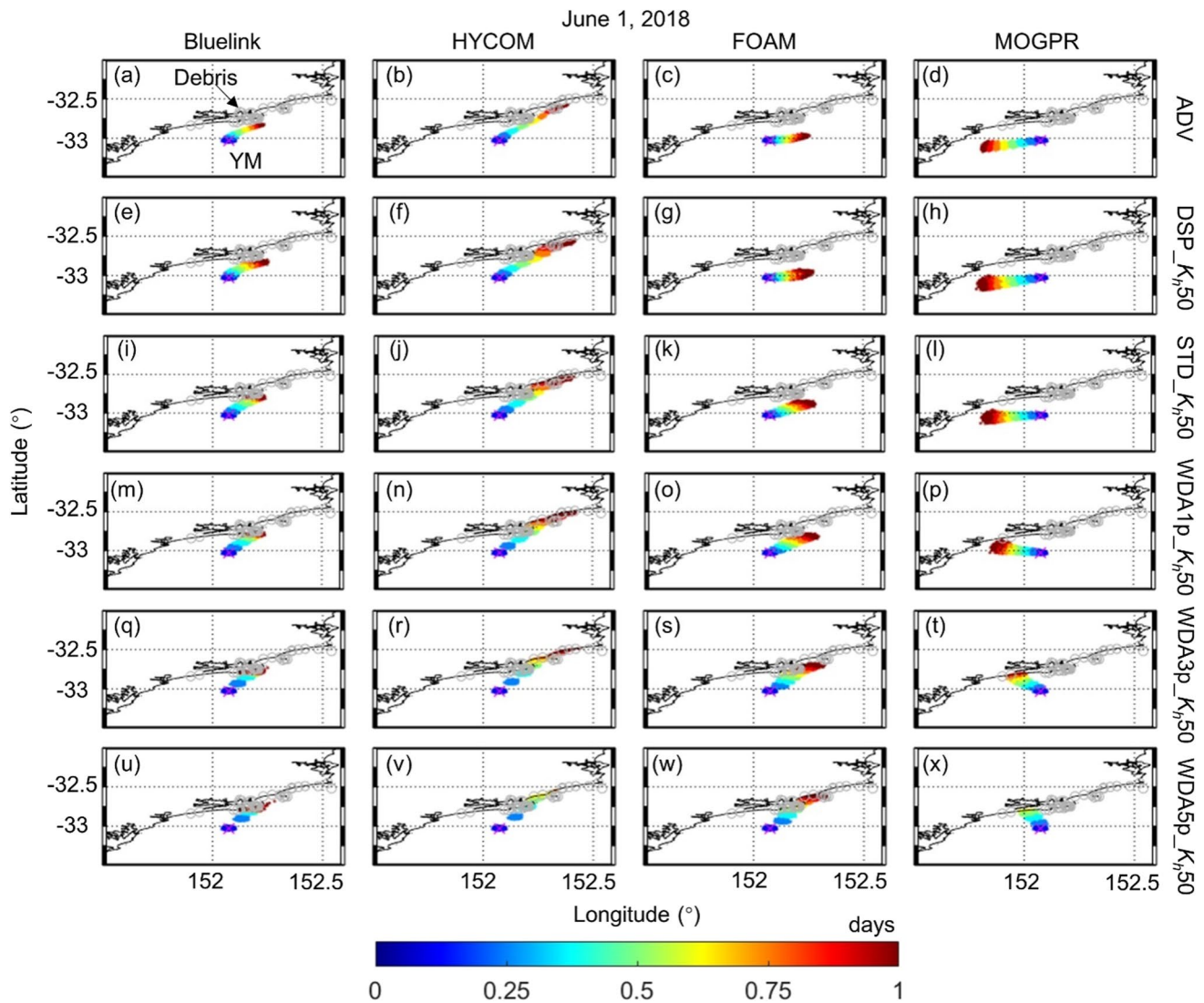


Fig. 4 Modelled particle trajectories under different forcings (ADV, DSP, STD and WDA) on June 1, 2018. From the left to right, it is results based on Bluelink, HYCOM, FOAM and MOGPR, respectively. From the top to bottom, it is the simulation ADV, DSP_ K_h50 , STD_ K_h50 , WDA1p_ K_h50 , WDA3p_ K_h50 and WDA5p_ K_h50 ,

respectively. For a better visualization, spotted debris is denoted by grey hollow circles. The colour at each trajectory point shows the time when the particles reached this grid. All panels have the same horizontal and vertical scales

spotted. The particle patterns can be easily explained by the surface current. In FOAM and MOGPR, the current near the shoreline is not well resolved due to the relatively coarse resolutions. For instance, the surface current direction on June 1 is south-westward in MOGPR (Fig. S1). There are no remarkable differences between cases ADV (1st row) and DSP_ K_h50 (2nd row), although particles were generally more dispersed and moved slightly faster when the horizontal dispersion was considered. The Stokes drift to some extent transported these particles towards the coastline, which can be inferred from the distribution of Stokes drift velocity on June 1, 2018 (Fig. 2b). The windage led more particles approach the coastal areas and

enter the domain where debris was spotted. For instance, under a strong windage ($\alpha = 5\%$), most debris move into the coastline in R3, R4 and R5 (Fig. 4u, v, w). Even using the MOGPR surface current, debris can enter the R2 under a moderate (Fig. 4t) or strong (Fig. 4x) windage forcing.

To determine how particle movement is sensitive to the horizontal dispersion strength, we compared simulations with different K_h (Fig. S2). On June 1, 2018, particles were generally more dispersed from each other under a stronger horizontal dispersion. In almost all cases, particles moved a longer distance when the horizontal dispersion was stronger. This is especially apparent under a large windage coefficient. For instance, particles mainly resided in

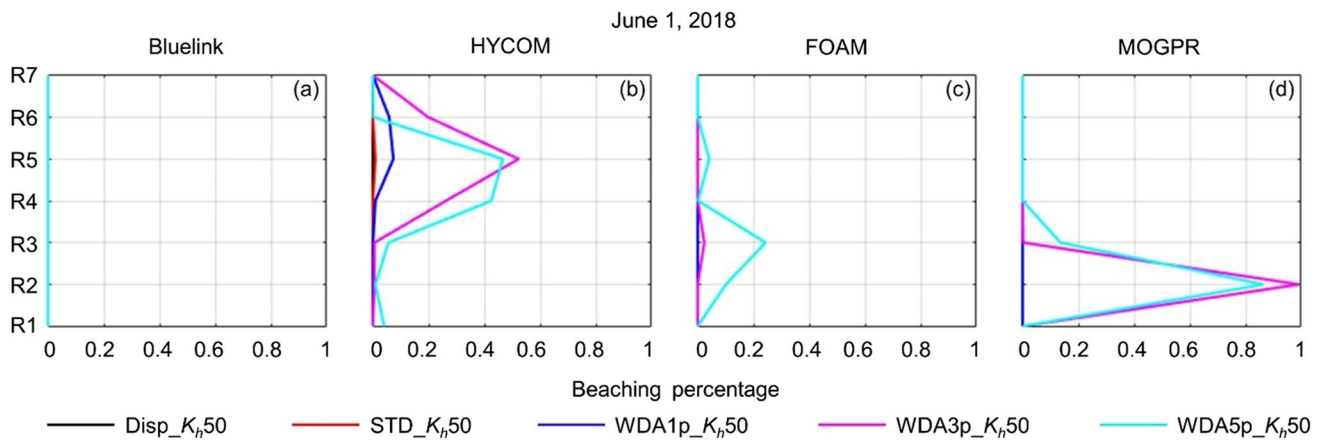


Fig. 5 Beaching percentage on June 1, 2018, in different cases. From the left to right, the surface current is from Bluelink, HYCOM, FOAM and MOGPR, respectively. Different colour lines are used to denote different cases. K_h is $50 \text{ m}^2/\text{s}$

R3 when the windage was strong but the horizontal dispersion was weak (Fig. S2q). When K_h increased to $200 \text{ m}^2/\text{s}$, some particles moved into R4 and R5 (Fig. S2t).

3.1.2 Beaching percentage in R1–R7

To have a quantitative comparison, we calculated the percentage of beached particles in R1–R7 along the coastline. On June 1, 2018, particles may beach when windage effects were considered (Fig. 5). We emphasize here again that the simulated beaching may only represent a chance of beaching, subject to the resolution of forcing. Beaching is not seen in the scenarios forced by the Bluelink surface current, but around half of the debris beached in R4 or R5 when forced by the HYCOM surface current along with a moderate ($\alpha=3\%$) or strong windage ($\alpha=5\%$). Under a strong windage ($\alpha=5\%$), there are around 20% of particles may beach in R3 when using FOAM surface current. MOGPR surface current, along with a moderate ($\alpha=3\%$) or strong windage ($\alpha=5\%$), lead to beaching of around almost 100% or 80% of particles on the first day, but mainly in R2. The available spatial patterns of the spotted debris shown in Fig. 1b cover the first 16 days after the YM incident, which means that we do not know how much debris reached the coastline on June 1, 2018, as we have no information of beaching time. However, according to the local news, some items found near Port Stephen (in R4) on June 1, 2018, were likely from the lost contains of YM.¹ Therefore, HYCOM may provide a better estimate of the surface current on June 1 than other datasets, and the role played by the windage cannot be ignored. This highlights the importance of resolving the small-scale coastal processes, although the spatial pattern of

surface current on June 1 is similar between Bluelink (Fig. S1a) and HYCOM (Fig. S1b).

Here is a short summary on the intercomparison between different simulations shown in Figs. 4 and 5. On the first day, the relative importance of physical processes on the particle distribution is case sensitive. In Bluelink and HYCOM, the surface current is the most important forcing for the particle movement; in FOAM and MOGPR, windage plays an important role. Compared to other surface current datasets, HYCOM leads to particles move farthest and particles were more uniformly distributed in the domain with spotted debris, and it may be the best estimate of the surface current on June 1 among the four datasets in this study, at least from the captured beaching in R4 on June 1.

3.2 During June 1–5, 2018

3.2.1 Spatial distribution of the released particles

When only forced by the Bluelink surface current, particles were almost confined to south of 32.5°S . However, under a strong windage ($\alpha=5\%$), some particles moved as far as 31.8°S (Fig. 6u). There was a significant directional change of these particles in R6, with most particles reversed towards to south-westward. However, the accuracy of this reverse highly depends on the accurate representation of small-scale nearshore processes, which may be beyond of a model with a resolution of 0.1° . When forcing TrackMPD with only HYCOM surface current, particles moved north-eastward into R3–R7 (Fig. 6b). Particles might move farther north when considering the horizontal dispersion (Fig. 6f). The overall spatial pattern of particle distribution is similar among DSP_ K_h50 , STD_ K_h50 and WDA1p_ K_h50 with the HYCOM surface current. Practical changes were noted when applying a moderate ($\alpha=3\%$) or

¹ <https://twitter.com/7newssydney/status/1002497557543596032>

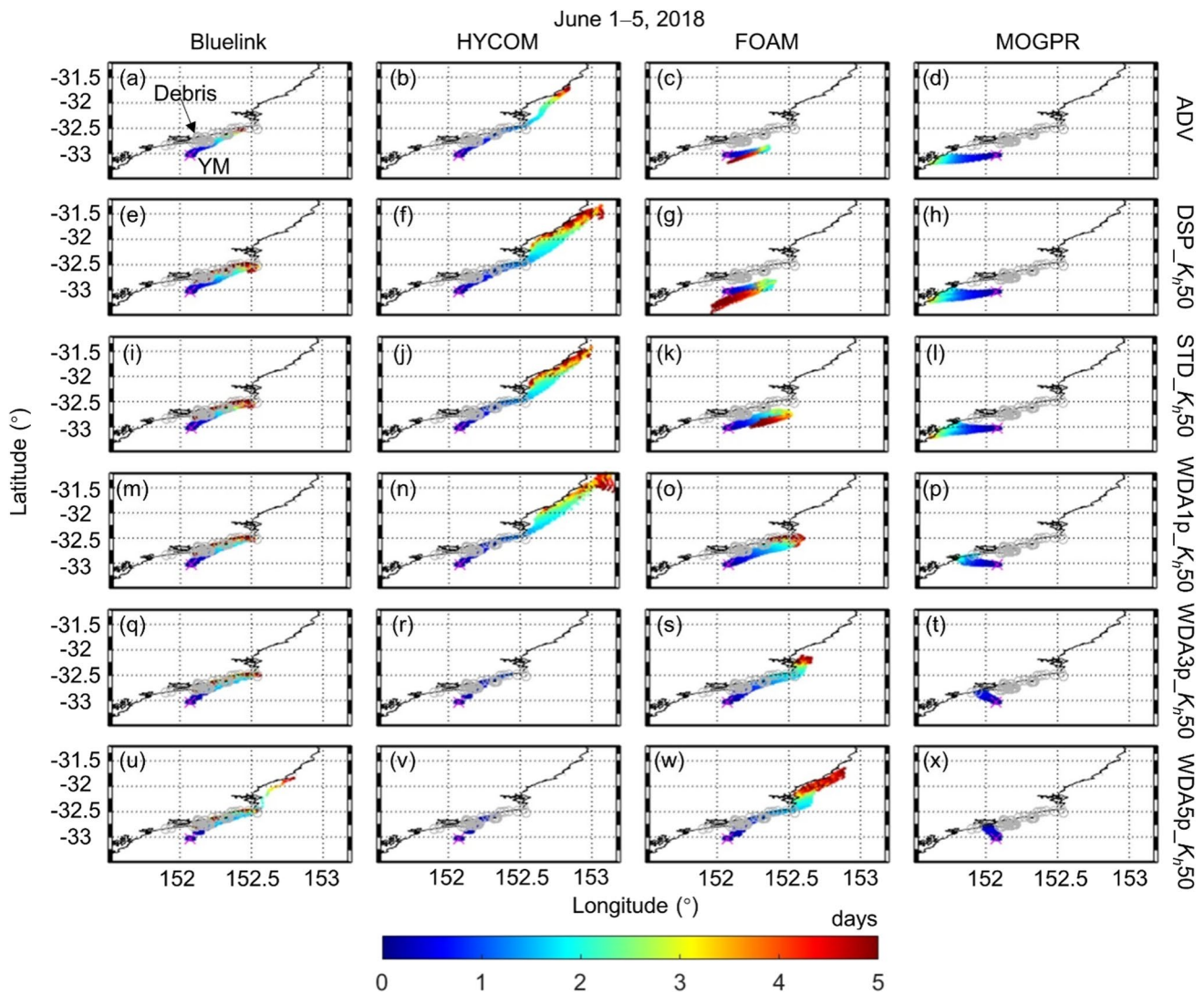


Fig. 6 As for Fig. 4 but over June 1–5, 2018

strong ($\alpha = 5\%$) windage impact. More specifically, all the particles were confined to 32.5°S , especially when the windage is strong. This suggests that the highly-buoyant debris was likely to beach near the Karuah River, and there must be some weakly-buoyant debris that reached farther north, corresponding to the debris spotted to the north of 32.5°S . With FOAM surface current only, particles approximately moved eastward during the first 2 days and then reversed to the south-westward direction (Fig. 6c), highly similar to the surface current direction (Fig. S1c, g). The horizontal dispersion considerably accelerated the particle movements, especially on June 4 and 5 (Fig. 6g). Since the Stokes-drift velocity was approximately in the northward direction during June 1–5, the particles were mostly confined to north of 32.5°S and their westward movements were significantly reduced (Fig. 6k). Since the windage was also in the northward direction, it further forced the particles northward and

prevented them from moving westward. Although beaching was seen in R6 and R7, there was no beaching in R4 on June 1, which contradicted with the report of local news. One can note that the beaching in R2 was not captured even with BlueLink or HYCOM surface current forcing, but we do not know whether the R2 beaching occurred before or after June 5, due to the unavailability of beaching time. It is clear that the trajectories forced by the MOGPR surface current were markedly different from trajectories forced by other surface currents (BlueLink, HYCOM and FOAM), even after inclusions of the horizontal dispersion (Fig. 6h), Stokes drift (Fig. 6l) and windage (Fig. 6p, t, x). This is primarily caused by the suboptimal representation of the surface current. For instance, the averaged surface current near the coastline was alongshore in the north-eastward direction in BlueLink and HYCOM, even in FOAM, but it was mainly south-westward or westward in MOGPR (Fig. S1h).

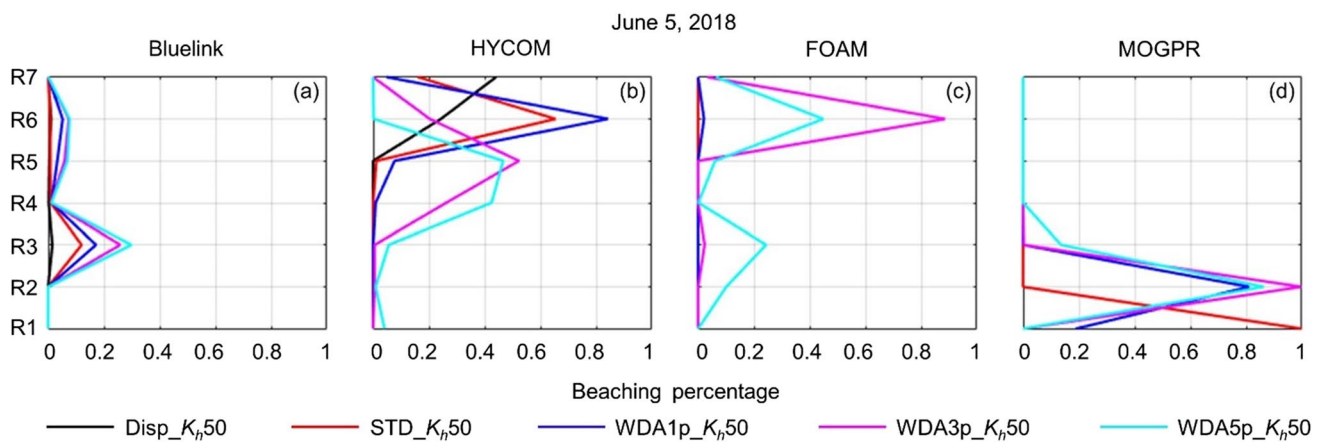


Fig. 7 Similar to Fig. 5 but on June 5, 2018

Over the first 5 days, particle trajectories might weakly depend on the horizontal dispersion when windage was excluded (Fig. S3). However, a moderate ($\alpha=3\%$) or strong ($\alpha=5\%$) windage could significantly impact the movements of particles. More specifically, under a weak horizontal dispersion, there was no any particle arriving north to 32.5°S by the end of June 5, 2018, in case WDA5p_Kh,5 with the Bluelink surface current (Fig. S3q). In case WDA5p_Kh,200, however, some particles could move much farther north to around 31.2°S (Fig. S3t).

3.2.2 Beaching percentage in R1–R7

Overall, by the end of June 5, 2018, particles might mostly beach in R3 when using Bluelink surface current, and beaching percentage in R3 increased with inclusion of Stokes drift and windage (Fig. 7a). More specifically, in STD_Kh,50, around 11% of particles beached in R3 by June 5, indicating that Stokes drift favours the onshore transport of particles (note the lack of Stokes drift data near the coastline). When the windage was strong ($\alpha=5\%$), the beaching percentage was around 28% in R3. The almost exclusive beaching in R3 is consistent with the spatial pattern of spotted debris, which also showed that R3 was a beaching hotspot (Fig. 1b). Additionally, particle beaching in R5 and R6 was only possible when the windage was included (Fig. 7a). The beaching in R4 (another hotspot) was completely missed (Fig. 7a), which was likely to be unrealistic according to the available spotted debris and the local news report. When the surface current was from HYCOM, more beaching was noted in R4–R6, whereas the beaching in R3 was almost invisible, except when the windage was strong ($\alpha=5\%$, Fig. 7b). It was observed that particle mainly beached in R4 and R5 when the windage was moderate ($\alpha=3\%$) or strong ($\alpha=5\%$), but mainly in R6 when the windage was weak or excluded. Observations showed that debris was mostly in R3–R6. That

means, the two eddy-resolving forecasts may provide a reasonable estimate of the surface current. Although beaching in R3 and R6 was simulated at moderate ($\alpha=3\%$) or strong ($\alpha=5\%$) windage, the failure in reproducing beaching in R4–5, along with the particle trajectories in Fig. 6, suggested that the FOAM surface current forecast may not be reasonable in our case. With the MOGPR surface current, beaching north of R3 was completely invisible. Combing with the particle trajectories, one can infer that the MOGPR surface current may be a suboptimal representation of the nearshore processes, and therefore may not be suitable for the debris tracking in coastal regions due to the relatively coarse resolution.

3.3 During June 1–16, 2018

3.3.1 Spatial distribution of the released particles

The spatial distribution of the large-scale surface current averaged over June 1–16 was similar between these datasets (Fig. S1). An anticyclonic eddy to the southeast of YM was captured in all these four datasets. The locations and extensions of major eddies were similar between these four datasets, despite of discernible differences. For instance, the eddy captured by MOGPR was slightly larger than the one captured by FOAM. From day 5 to day 16, some particles might be trapped by adjacent eddies when using Bluelink or FOAM surface current (Fig. 8). For example, under a moderate ($\alpha=3\%$) or strong ($\alpha=5\%$) windage, some particles were trapped by the anticyclonic mesoscale eddy (green arrow in Fig. 2g) southeast to YM site and some particles might flow with the separated EAC (light blue arrow in Fig. 2g). The eddy trapping at moderate ($\alpha=3\%$) or strong ($\alpha=5\%$) windage was because windage forced particles to R4 and R5 when the surface current was from Bluelink, and these particles were subsequently

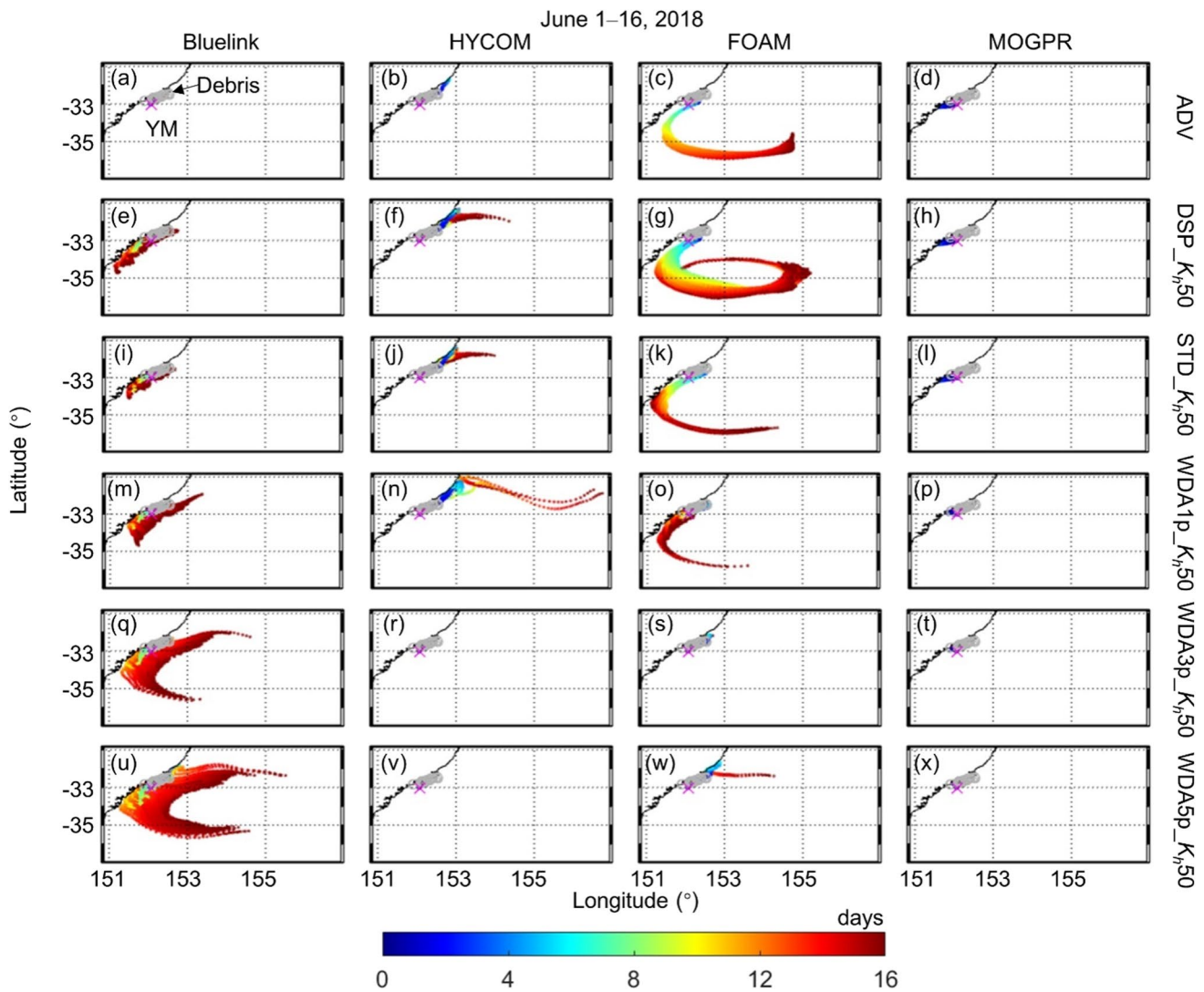


Fig. 8 As for Fig. 4 but over June 1–16, 2018

brought by the south-westward flow to the eddy periphery. In contrast, the eddy trapping only occurred when the windage was excluded or weak if the surface current was from FOAM. This is because a strong northward windage would force the particles northward to R6, when the surface current was from FOAM, and there was therefore a very low chance for particles to encounter the mesoscale eddy to the southeast of YM. Under the forcing of HYCOM surface current, most particles beached during the first 5 days (Fig. 7) and therefore very few particles could encounter the mesoscale eddy. However, when using HYCOM surface current, some particles might enter the separated EAC when ignoring or applying a weak windage. As shown in Fig. 7, almost all the particles beached in R1 or R2 during the first 5 days when the surface current was from MOGPR, and therefore no eddy trapping was noticed.

3.3.2 Beaching percentage in R1–R7

Since the available spotted debris shown in this study was collected during the first 16 days, a reliable debris forecast should reproduce a beaching pattern similar to the spotted debris during June 1–16, 2018. Overall, the Bluelink surface current, when combined with Stokes drift and windage, could reproduce the beaching in R3–R6, and R3 accounted for more beaching than other regions (Fig. 9a). However, we cannot estimate the beaching percentage in each region from the spotted debris, as the spotted debris only showed the qualitative but not quantitative spatial distribution. Comparing Fig. 9a with Fig. 7a, one can note that a comparable beaching was finished during the first 5 days and during June 5–16, respectively, when the Bluelink surface current was applied. The Bluelink surface current could not reproduce the beaching in R2 (Fig. 9a). The concentrated beaching in

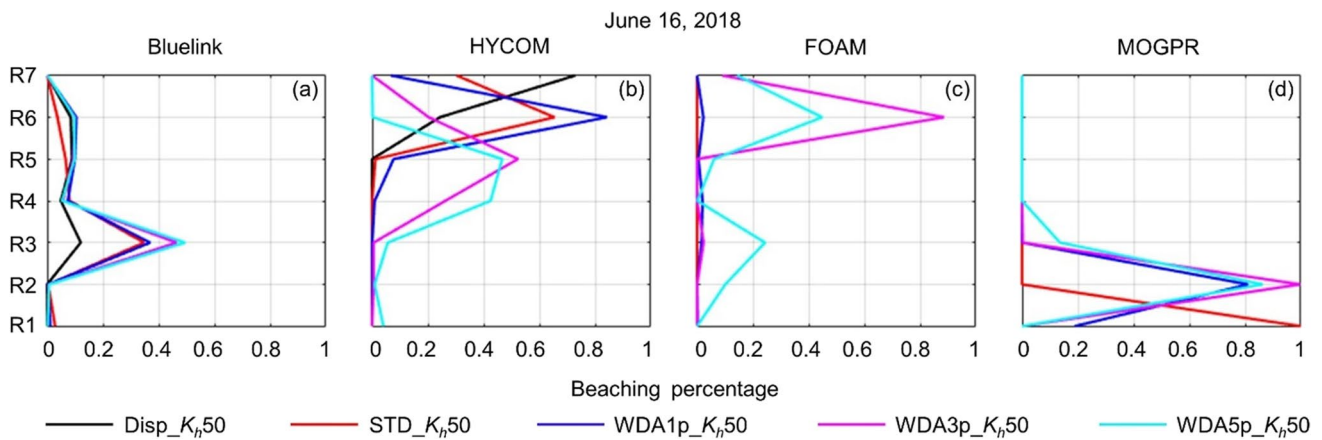


Fig. 9 Similar to Fig. 5 but on June 16, 2018

R4–R6 was simulated with the HYCOM surface current, which roughly agreed with the spatial pattern of spotted debris. However, beaching was quite low in R3 and was completely invisible in R2 (Fig. 9b). Therefore, this suggests that debris forecast based on multiple forcing datasets may need to be combined to have a more comprehensive forecast. Comparing Fig. 9b with Fig. 7b indicates beaching was finished in the first 5 days when forced by the HYCOM surface current. Forecast with FORMA surface current could reproduce the concentrated beaching in R6 at moderate ($\alpha=3\%$) or strong ($\alpha=5\%$) windage, and beaching in R3 was mainly seen at strong ($\alpha=5\%$) windage. Beaching in R2, R4 and R5 (except when $\alpha=5\%$) was not reproduced by the FOAM surface current. Similar to the scenarios forced by the HYCOM surface current, beaching was almost finished in the first 5 days when forced by FOAM surface current. It is clear that beaching significantly differed from observations in the scenarios forced by MOGPR surface current.

4 Conclusions and discussion

A framework was built for the purpose of forecast of floating marine debris from ship containers. By comparing simulated particle distribution patterns with observations, the principal findings are summarized as follows.

- (1) The forecast framework could approximately reproduce the observed patterns of debris when applying an eddy-resolving surface-current forecast, along with the horizontal dispersion, Stokes drift and windage. In principle, the surface current determines the large-scale overall patterns of debris trajectories. Significant differences were observed when using different surface-current datasets. Bluelink surface current reproduced beaching in R3, whilst HYCOM surface current had a

- better performance in R4–R6. In addition, beaching in R2 was simulated when using FOAM surface current. This implies different datasets had different strengths and weaknesses.
- (2) The windage may be the second important factor in the debris movements, at least in our simulation. A strong ($\alpha=5\%$) windage could significantly modulate the debris trajectories and fates, especially in a longer period (16 days in this study). Even on the first day, a moderate ($\alpha=3\%$) or strong ($\alpha=5\%$) windage could produce practical differences to the simulated debris trajectories.
- (3) The horizontal dispersion can be used to parametrize the unresolved small-scale processes. Strong horizontal dispersion could significantly impact the debris trajectories. Stokes drift played a minor role in the transport of marine debris from YM incident when Bluelink or HYCOM surface current was used, but could play a greater role when using FOAM or MOGPR surface current.

To the best of our knowledge, there has been very limited attention on MPD from lost containers in the ocean, with real-world observations available for validation. Although we compared our simulations to the available observations of debris from YM, we acknowledge that the available observations used in this paper are far from being sufficient. For instance, comparing both the location and time of beaching of different buoyant objects can make the study more interesting and convincing. A similar but more detailed case study is therefore expected if the required information is available. Nonetheless, our work provides an efficient forecast procedure for floating debris spill from lost containers and demonstrates that forcing TrackMPD with some operational forecast data is viable for debris transport forecast. Similar simulations can help to estimate when, where and

how much debris will beach once containers spill from a cargo ship, thereby assisting clean-up efforts for similar marine incidents in the future.

We also showed that the choice of K_h can be important to affect beaching prediction, and this sensitivity to K_h value precisely reflects the model's shortcoming determined by its coarse resolution. The importance of our work is to show that the subgrid-scale processes, such as sub-mesoscale eddies or other coastal processes not resolved by currently available global forecast models, are important for debris transport and beaching. Where these are unknown, our work has shown that these subgrid-scale processes can be approximated by the horizontal dispersion (in 2D cases), if necessary and provided reasonable approximations. Although our models showed good performance, more work is expected to further improve its forecast ability. This includes, but is not limited to, applying a coupled current-wave model results. Also highly desirable are in situ measurements of horizontal diffusivity (e.g. using real-time drifters). In addition, a higher temporal resolution of the forcing is also expected, and impacts from sub-mesoscale structures may also be identified. Furthermore, a 3D simulation may reveal more details.

Presumably, forcing from a regional model with a much higher resolution may improve the simulation accuracy. However, we recognize the fact that a marine-debris spill like the YM incident may occur in any oceans at any time. Not always will a suitable regional ultra-high-resolution forecast model covering the debris spill and the potential spread of the spill debris be available. Therefore, a global operational forecast data, like what used here, may be a reasonable choice for forecasting movement of marine debris for an actual marine incident. It would be interesting to test the framework here in other waters, so that a quick and reliable forecast can be conducted once a similar marine incident occurs. Although beyond the scope of this work, we expect to see more extensive intercomparisons and tests of both the current particle tracking tools (e.g. TrackMPD and OpenDrift (Dagestad et al. 2018)) and operational oceanic and atmospheric forecasts in coastal waters where marine incident that generate actual debris fields are likely. Not only will these generate (unfortunately) actual debris fields that can be observed and tracked, they will also make it clearer what tools and data to be used for forecast purpose in a given water domain, should similar marine debris incidents occur. And given the prevalence of flood-related, non-maritime, point source pollution incidents (plastic rafts from river mouths) the application of these models may also assist in predicting where those debris could collect or come ashore, adding power and confidence to the use of the models in less certain contexts.

This study was motivated by the increasing marine incidents like YM and the insufficient attention found in the

literature. Although we made an attempt to build a forecast framework in this study, it by no means conveys the message that this work is applicable to all other marine incidents. Just as the performance differences between Bluelink and HYCOM, it is necessary to consider multiple forcing datasets to evaluate their performance in a specific scenario. Although we found that a horizontal resolution of 0.25° may be too coarse for our debris forecast, it does not necessarily mean that such a resolution is not applicable in other debris forecast. In one word, our work may be more of an example in forecasting marine debris spilled from lost containers. It may provide an applicable procedure in marine debris forecast, but the forcing performance, and the relative importance of different physical processes may be highly case sensitive.

Supplementary Information The online version contains supplementary material available at <https://doi.org/10.1007/s10236-023-01539-x>.

Acknowledgements Fanglou Liao was supported by the China Scholarship Council and a UNSW Canberra Top-up Scholarship. The authors thank the Australian Bureau of Meteorology for providing the wave data, NOAA/NCEP for public access to the wind data, and the public access to the surface current datasets. Dr Peter McIntyre kindly helped to improve the manuscript. This is publication no. 80 of the Sino-Australian Research Consortium for Coastal Management (previously the Sino-Australian Research Centre for Coastal Management).

TrackMPD: <https://github.com/IJalonRojas/TrackMPD>. Bluelink forecast data: http://opendap.bom.gov.au:8080/thredds/dodsC/ocean_maps_an_datasets/. HYCOM forecast data: https://tds.hycom.org/thredds/catalogs/GLBv0.08/expt_93.0.html. FOAM forecast data: https://resources.marine.copernicus.eu/product-detail/GLOBAL_ANALYSIS_FORECAST_PHY_CPL_001_015_INFORMATION. MOGPR dataset: https://resources.marine.copernicus.eu/product-detail/MULTI_OBS_GLO_PHY_REP_015_004. Significant wave height and Stokes drift velocity: http://opendap.bom.gov.au:8080/thredds/catalogs/paccs_ap-catalog.html. Forecast wind velocity data: https://www.pacioos.hawaii.edu/metadata/ncep_global.html.

Declarations

Competing interests The authors declare no competing interests.

References

- Abascal AJ, Castanedo S, Mendez FJ, Medina R, Losada IJ (2009) Calibration of a Lagrangian transport model using drifting buoys deployed during the Prestige oil spill. *J Coastal Res* 25:80–90. <https://doi.org/10.2112/07-0849.1>
- Anderson Eric et al (1998) Modeling of leeway drift. Final report September 1998. Report No. CG-D-06–99. U.S. Coast Guard Research and development Center
- Australian Transport Safety Bureau (2020) Loss of containers overboard from YM Efficiency. Australian Maritime Safety Authority Annual Report 2018–19
- ASCE Task Committee on Modeling of Oil Spills of the Water Resources Engineering Division (1996) State-of-the-art review of modeling transport and fate of oil spills. *J Hydraulic Eng*

- 122, 594–609. [https://doi.org/10.1061/\(ASCE\)0733-9429\(1996\)122:11\(594\)](https://doi.org/10.1061/(ASCE)0733-9429(1996)122:11(594))
- Barnes DK, Galgani F, Thompson RC, Barlaz M (2009) Accumulation and fragmentation of plastic debris in global environments. *Philos Trans R Soc B* 364:1985–1998. <https://doi.org/10.1098/rstb.2008.0205>
- Beegle-Krause CJ (2001) General NOAA Oil Modeling Environment GNOME: a new spill trajectory model. IOSC 2001 proceedings; Tampa. March 26–29; St. Louis, MO: Mira Digital Publishing, Inc. 2: 865–871. <https://doi.org/10.7901/2169-3358-2001-2-865>
- Blockley EW, Martin MJ, McLaren AJ, Ryan AG, Waters J, Lea DJ, Mirouze I, Peterson KA, Sellar A, Storkey D (2014) Recent development of the Met Office operational ocean forecasting system: an overview and assessment of the new Global FOAM forecasts. *Geoscientific Model Development* 7:2613–2638. <https://doi.org/10.5194/gmd-7-2613-2014>
- Brassington G, Pugh T, Spillman CM, Schulz E, Beggs H, Schiller A, Oke PR (2007) BLUElink > development of operational oceanography and servicing in Australia. *J Res Pract Inf Technol* 39:151–164
- Bravo M, de los Angeles Gallardo M, Luna-Jorquera G, Núñez P, Vásquez N, Thiel M (2009) Anthropogenic debris on beaches in the SE Pacific (Chile): results from a national survey supported by volunteers. *Marine Pollut Bull* 58, 1718–1726. <https://doi.org/10.1016/j.marpolbul.2009.06.017>
- Breivik Ø, Allen AA (2008) An operational search and rescue model for the Norwegian Sea and the North Sea. *J Mar Syst* 69:99–113. <https://doi.org/10.1016/j.jmarsys.2007.02.010>
- Breivik Ø, Allen AA, Maisondieu C, Roth JC (2011) Wind-induced drift of objects at sea: the leeway field method. *Appl Ocean Res* 33:100–109. <https://doi.org/10.1016/j.apor.2011.01.005>
- Browne MA, Galloway T, Thompson R (2009) Microplastic—an emerging contaminant of potential concern? *Integr Environ Assess Manag* 3:559–561. <https://doi.org/10.1002/ieam.5630030412>
- Brushett BA, King BA, Lemckert CJ (2016) Assessment of ocean forecast models for search area prediction in the eastern Indian Ocean. *Ocean Model* 97:1–15. <https://doi.org/10.1016/j.ocemod.2015.11.002>
- Carson HS, Lamson MR, Nakashima D, Toloumu D, Hafner J, Maximenko N, Mcdermid KJ (2013) Tracking the sources and sinks of local marine debris in Hawai'i. *Mar Environ Res* 84:76–83. <https://doi.org/10.1016/j.marenvres.2012.12.002>
- Carlson D, Fredj E, Gildor H, Rom-Kedar V (2010) Deducing an upper bound to the horizontal eddy diffusivity using a stochastic Lagrangian model. *Environ Fluid Mech* 10:499–520. <https://doi.org/10.1007/s10652-010-9181-0>
- Critchell K, Grech A, Schlaefer JA, Andutta FP, Lambrechts J, Wolanski E, Hamann M (2015) Modelling the fate of marine debris along a complex shoreline: lessons from the Great Barrier Reef. *Estuar Coast Shelf Sci* 167:414–426. <https://doi.org/10.1016/j.ecss.2015.10.018>
- Critchell K, Lambrechts J (2016) Modelling accumulation of marine plastics in the coastal zone; what are the dominant physical processes? *Estuar Coast Shelf Sci* 171:111–122. <https://doi.org/10.1016/j.ecss.2016.01.036>
- Critchell K, Bauer-Civiello A, Benham C, Berry K, Eagle L, Hamann M, Hussey K, Ridgway T (2019) Chapter 34 - plastic pollution in the coastal environment: current challenges and future solutions, in: Wolanski, E., Day, J.W., Elliott, M., Ramachandran, R. (Eds.), *Coasts and estuaries*. Elsevier, pp. 595–609. <https://doi.org/10.1016/B978-0-12-814003-1.00034-4>
- Cummings JA (2005) Operational multivariate ocean data assimilation. *Q J R Meteorol Soc* 131:3583–3604. <https://doi.org/10.1256/qj.05.105>
- Cummings JA, Smedstad OM (2013) Variational data assimilation for the global ocean. In: Park S., Xu L. (eds) *Data assimilation for atmospheric, oceanic and hydrologic applications* (Vol. II). Springer, Berlin, Heidelberg. https://doi.org/10.1007/978-3-642-35088-7_13
- Dagestad K-F, Röhrs J, Breivik Ø, Ådlandsvik B (2018) OpenDrift v1.0: a generic framework for trajectory modelling. *Geoscientific Model Development* 11:1405–1420. <https://doi.org/10.5194/gmd-11-1405-2018>
- Derraik JG (2002) The pollution of the marine environment by plastic debris: a review. *Mar Pollut Bull* 449:842–852. [https://doi.org/10.1016/S0025-326X\(02\)00220-5](https://doi.org/10.1016/S0025-326X(02)00220-5)
- Díaz-Torres ER, Ortega-Ortiz CD, Silva-Iñiguez L, Nene-Preciado A, Orozco ET (2017) Floating marine debris in waters of the Mexican Central Pacific. *Mar Pollut Bull* 115:225–232. <https://doi.org/10.1016/j.marpolbul.2016.11.065>
- Dobler D, Huck T, Maes C, Grima N, Blanke B, Martinez E, Arduin F (2019) Large impact of Stokes drift on the fate of surface floating debris in the South Indian Basin. *Mar Pollut Bull* 148:202–209. <https://doi.org/10.1016/j.marpolbul.2019.07.057>
- Durrant T, Greenslade D, Hemer M, Trenham C (2014) A global wave hindcast focussed on the Central and South Pacific. CAWCR Technical Report No. 070
- Ebbesmeyer CC, Ingraham W, Jones JA, Donohue MJ (2012) Marine debris from the Oregon Dungeness crab fishery recovered in the northwestern Hawaiian Islands: identification and oceanic drift paths. *Mar Pollut Bull* 65:69–75. <https://doi.org/10.1016/j.marpolbul.2011.09.037>
- González-Fernández D, Hanke G (2017) Toward a harmonized approach for monitoring of riverine floating macro litter inputs to the marine environment. *Front Mar Sci* 4:86. <https://doi.org/10.3389/fmars.2017.00086>
- Harris PT (2020) The fate of microplastic in marine sedimentary environments: a review and synthesis. *Marine Pollut Bull* 158, 111398. <https://doi.org/10.1016/j.marpolbul.2020.111398>
- Helber RW, Townsend TL, Barron CN, Dastugue JM, Carnes MR (2013) Validation test report for the Improved Synthetic Ocean Profile (ISOP) system, part i: synthetic profile methods and algorithm. NRL Memo. Report, NRL/MR/7320-13-9364
- Hemer MA, Zieger S, Durrant T, O'Grady J, Hoeke RK, McInnes KL, Rosebrock U (2017) A revised assessment of Australia's national wave energy resource. *Renewable Energy* 114:85–107. <https://doi.org/10.1016/j.renene.2016.08.039>
- Jalón-Rojas I, Wang X-H, Fredj E (2019a) Technical note: on the importance of a three-dimensional approach for modelling the transport of neustic microplastics. *Ocean Sci Discussions*. 15(3). <https://doi.org/10.5194/os-15-717-2019>
- Jalón-Rojas I, Wang XH, Fredj E (2019b) A 3D numerical model to Track Marine Plastic Debris (TrackMPD): sensitivity of microplastic trajectories and fates to particle dynamical properties and physical processes. *Mar Pollut Bull* 141:256–272. <https://doi.org/10.1016/j.marpolbul.2019.02.052>
- Jambeck JR, Geyer R, Wilcox C, Siegler TR, Perryman M, Andrady A, Narayan R, Law KL (2015) Plastic waste inputs from land into the ocean. *Science* 347:768–771. <https://doi.org/10.1126/science.1260352>
- Kako SI, Isobe A, Kataoka T, Hinata H (2014) A decadal prediction of the quantity of plastic marine debris littered on beaches of the East Asian marginal seas. *Marine Pollut Bull* 81, 174–184. <https://doi.org/10.1016/j.marpolbul.2014.01.057>
- Keswani A, Oliver DM, Gutierrez T, Quilliam RS (2016) Microbial hitchhikers on marine plastic debris: human exposure risks at bathing waters and beach environments. *Mar Environ Res* 118:10–19. <https://doi.org/10.1016/j.marenvres.2016.04.006>
- Lea DJ, Mirouze I, Martin MJ, King RR, Hines A, Walters D, Thurlow M (2015) Assessing a new coupled data assimilation system based on the Met Office coupled atmosphere–land–ocean–sea

- ice model. *Mon Weather Rev* 143:4678–4694. <https://doi.org/10.1175/MWR-D-15-0174.1>
- Lebreton L-M, Greer S, Borrero JC (2012) Numerical modelling of floating debris in the world's oceans. *Mar Pollut Bull* 64:653–661. <https://doi.org/10.1016/j.marpolbul.2011.10.027>
- Lebreton LCM, Van der Zwet J, Damsteeg JW, Slat B, Andrady A, Reisser J (2017) River plastic emissions to the world's oceans. *Nat Commun* 8:15611. <https://doi.org/10.1038/ncomms15611>
- Lermusiaux PFJ, Doshi M, Kulkarni CS, Gupta A, Haley PJ, Mirabito C, Trotta F, Levang SJ, Flierl GR, Marshall J, Peacock T, Noble C (2019) Plastic pollution in the coastal oceans: characterization and modeling, in: OCEANS 2019 MTS/IEEE SEATTLE. Presented at the OCEANS 2019 MTS/IEEE SEATTLE, pp. 1–10. <https://doi.org/10.23919/OCEANS40490.2019.8962786>
- Oke PR, Griffin D, Schiller A, Matear RJ, Fiedler R, Mansbridge JV, Lenton A, Cahill M, Chamberlain M, Ridgway KR (2012) Evaluation of a near-global eddy-resolving ocean model. *Geoscientific Model Development* 6:591–615. <https://doi.org/10.5194/gmd-6-591-2013>
- Okubo A (1971) Oceanic diffusion diagrams. *Deep-Sea Res Oceanogr Abstr* 18:789–802. [https://doi.org/10.1016/0011-7471\(71\)90046-5](https://doi.org/10.1016/0011-7471(71)90046-5)
- Onink V, Wichmann D, Delandmeter P, Van Sebille E (2018) The role of Ekman currents, geostrophy and Stokes drift in the accumulation of floating microplastic. *Journal of Geophysical Research: Oceans* 124(3):1474–1490. <https://doi.org/10.1029/2018JC014547>
- Peliz A, Marchesiello P, Dubert J, Marta-Almeida M, Roy C, Queiroga H (2007) A study of crab larvae dispersal on the Western Iberian Shelf: physical processes. *J Mar Syst* 68:215–236. <https://doi.org/10.1016/j.jmarsys.2006.11.007>
- Rochman CM, Tahir A, Williams SL, Baxa DV, Lam R, Miller JT, Teh FC, Werorilangi S, Teh SJ (2015) Anthropogenic debris in seafood: plastic debris and fibers from textiles in fish and bivalves sold for human consumption. *Sci Rep* 5:14340. <https://doi.org/10.1038/srep14340>
- Saha S, Moorthi S, Pan H-L, Wu X, Wang J, Nadiga S, Tripp P, Kistler R, Woollen J, Behringer D, Liu H, Stokes D, Grumbine R, Gayno G, Wang J, Hou Y, Chuang Y, Juang HH, Sela J, Iredell M, Kleist DT, Delst PV, Keyser D, Derber J, Ek M, Meng J, Wei H, Yang R, Lord SJ, Van Den Dool HM, Kumar A, Wang W, Long CS, Chelliah M, Xue Y, Huang B, Schemm JE, Ebisuzaki W, Lin R, Xie P, Chen M, Zhou S, Higgins W, Zou C, Liu Q, Chen Y, Han Y, Cucurull L, Reynolds RW, Rutledge G, Goldberg M (2010) The NCEP climate forecast system reanalysis. *Bull Am Meteor Soc* 91(8):1015–1058. <https://doi.org/10.1175/2010BAMS3001.1>
- Saha S, Moorthi S, Wu X, Wang J, Nadiga S, Tripp P, Behringer D, Hou Y, Chuang Y, Iredell MD, Ek M, Meng J, Yang R, Mendez M, Van Den Dool HM, Zhang Q, Wang W, Chen M, Becker E (2014) The NCEP climate forecast system version 2. *J Clim* 27(6):2185–2208. <https://doi.org/10.1175/JCLI-D-12-00823.1>
- Schmidt C, Krauth T, Wagner S (2017) Export of plastic debris by rivers into the sea. *Environ Sci Technol* 51(21):12246–12253. <https://doi.org/10.1021/acs.est.7b02368>
- Smagorinsky J (1963) General circulation experiments with the primitive equations: I. The Basic Experiment *Monthly Weather Review* 91(3):99–164. [https://doi.org/10.1175/1520-0493\(1963\)091%3c0099:GCEWTP%3e2.3.CO;2](https://doi.org/10.1175/1520-0493(1963)091%3c0099:GCEWTP%3e2.3.CO;2)
- Trinanes J, Olascoaga MJ, Goni G, Maximenko N, Griffin D, Hafner JJ (2016) Analysis of flight MH370 potential debris trajectories using ocean observations and numerical model results. *Journal of Operational Oceanography* 9:126–138. <https://doi.org/10.1080/1755876X.2016.1248149>
- United Nations Environmental Programme (2022) End plastic pollution: towards an international legally binding instrument. <https://wedocs.unep.org/20.500.11822/38525>
- van der Mheen M, Pattiaratchi C, van Sebille E (2019) Role of Indian Ocean dynamics on accumulation of buoyant debris. *Journal of Geophysical Research: Oceans* 124:2571–2590. <https://doi.org/10.1029/2018JC014806>
- Van Sebille E, Delandmeter P, Schofield J, Hardesty BD, Jones J, Donnelly A (2019) Basin-scale sources and pathways of microplastic that ends up in the Galápagos Archipelago. *Ocean Sci* 15:1341–1349. <https://doi.org/10.5194/os-15-1341-2019>
- Yoon J-H, Kawano S, Igawa S (2010) Modeling of marine litter drift and beaching in the Japan Sea. *Mar Pollut Bull* 60:448–463. <https://doi.org/10.1016/j.marpolbul.2009.09.033>
- Zhang H (2017) Transport of microplastics in coastal seas. *Estuar Coast Shelf Sci* 199:74–86. <https://doi.org/10.1016/j.ecss.2017.09.032>

Springer Nature or its licensor (e.g. a society or other partner) holds exclusive rights to this article under a publishing agreement with the author(s) or other rightsholder(s); author self-archiving of the accepted manuscript version of this article is solely governed by the terms of such publishing agreement and applicable law.